Cellulose (2021) 28:8355–8374
https://doi.org/10.1007/s10570-021-04063-7

ORIGINAL RESEARCH

# Synthesis of novel heterocyclic compounds based on dialdehyde cellulose: characterization, antimicrobial, antitumor activity, molecular dynamics simulation and target identification

**Mohamed Hasanin · Amr H. Hashem · Ahmed A. El-Rashedy · Samir Kamel**

Received: 8 February 2021 / Accepted: 3 July 2021 / Published online: 18 July 2021


**Abstract** In this study, new amino heterocyclic cellulose derivatives were prepared. Dialdehyde cellulose was functionalized by Schiff base reaction with (E)-2-(4-(dimethylamino) benzylidene)-4-oxo-4-phenylbutanehydrazide, (E)-2-((1,3-diphenyl-1H-pyrazol-4-yl)-4-oxo-4-phenylbutane hydrazide, and thiophene-2-carbohydrazide. The prepared derivatives were characterized and confirmed by Fourier-transform infrared spectroscopy, scanning electron microscopy, energy-dispersive X-ray, and Thermo gravimetric analysis. Additionally, antimicrobial activity of all derivatives was assessed as well as antitumor activity. Results revealed that, all derivatives have potential antimicrobial activity against *Escherichia coli, Pseudomonas aeruginosa*, *Staphylococcus aureus*, *Bacillus subtilis*, *Candida albicans, Cryptococcus neoformance, Aspergillus niger, A. fumigatus.* Additionally, (E)-2-(4-(dimethylamino) benzylidene)-4-oxo-4-phenylbutanehydrazide and (E)-2-((1,3-diphenyl-1H-pyrazol-4-yl)-4-oxo-4-phenylbutanehydrazide cellulose compounds have good antitumor activities against Hep G2 and MCF7 cancerous cell lines without any effects on Wi38 normal cell line. Molecular dynamics study revealed that (E)-2-(4-(dimethylamino) benzylidene)-4-oxo-4-phenylbutanehydrazide and (E)-2-((1,3-diphenyl-1H-pyrazol-4-yl)-4-oxo-4-phenylbutanehydrazide cellulose derivatives have selectively target the ATP binding pocket residues. Identification of these ATP binding site residues and their crucial roles could provide the structure basis for understanding c-Kit kinase auto-inhibition

**Keywords** Cellulose · Periodate oxidation · 2,3-Dialdehyde cellulose · Antimicrobial · Antitumor · Heterocyclic derivatives · Docking study

M. Hasanin (✉) · S. Kamel
Cellulose and Paper Department, National Research Centre, 33 El-Bohouth St. (Former El-Tahrir St.), P.O. 12622, Dokki, Giza, Egypt
e-mail: sido_sci@yahoo.com

A. H. Hashem (✉)
Botany and Microbiology Department, Faculty of Science, Al-Azhar University, Cairo 11884, Egypt
e-mail: amr.hosny86@azhar.edu.eg

A. A. El-Rashedy
Natural and Microbial Products Department, National Research Center, 33 El-Bohouth St. (Former El-Tahrir St.), P.O. 12622, Dokki, Giza, Egypt

## Introduction

Cancer is one of the most life-threatening diseases, with more than 100 different types occurring due to some molecular changes within the cell. It is the third leading cause of death worldwide following cardiovascular and infectious diseases (Kelloff 1999). Cancer is a multistage or multi mechanism procedure leading to the uncontrolled proliferation of abnormal

cells due to aberrations in numerous cell signaling circuits (Sung et al. 2012). The tumors and secondary infections especially in cancer patients are the first causes of mortality and morbidity over all the World (Siegel et al. 2015). Unfortunately, the most anticancer agents not necessarily have antimicrobial activity. In fact, the secondary infections by microorganisms in immune suppressed patients (usually cancer patients) in many cases are severing (de Coaña et al. 2015; Elbahnasawy et al. 2021). Therefore, the dual effect agents which have anticancer activity and antimicrobial activity are preferred in medical applications (Felício et al. 2017; Muthukumar et al. 2016). Moreover, due to lack of effective drugs, cost of chemotherapeutic agents, and the side effects of anticancer drugs, cancer can be a cause of death. Therefore, synthesis of new compounds have anticancer and antimicrobial is required, these compounds it must be effective, cheap and safe.

Cellulose derivatives are popular in medical application as carriers, filers, additives, stabilizer, thickness agents and ect (Ciechanska 2004; Hoenich 2006). Cellulose and its derivatives are characteristic by high safety profile materials (Abu-Elghait et al. 2021; El-Naggar et al. 2020; Hasanin et al. 2019; Hasanin and Moustafa 2020). Hence, there are used in many pharmaceutical industrial applications (Abdelraof et al. 2019a, 2019b, 2020). Moreover, the functionalized cellulosic materials now are targeted in pharmacopeia of drug preparations. DAC is one of the most attractive materials to use in drug formulation. Additionally, the DAC is the functionalized cellulose derivative with high reactivity as well as nontoxic, biodegradable and biocompatible (Dacrory et al. 2020). This study aimed to synthesize new heterocyclic cellulose derivatives through the Schiff's base reaction of TEMPO oxidized cellulose with some heterocyclic compounds. The structure of the prepared derivatives will be characterized by FTIR, TGA, SEM, and EDX analysis. The antimicrobial, antitumor, cytotoxicity, as well as molecular docking and dynamics prediction of the binding mode of the active compounds has been explored. This study illustrates an insight on the molecular properties of the lead compounds as potential inhibitors as well as the binding mode and contribution of the important residues at the active sites necessary for interaction of these identified inhibitors.

## Materials and method

### Materials

Bleached Kraft bagasse pulp was obtained from Misr Edfu Pulp, Writing & Printing Paper Company (MEPP Co.), Egypt. The chemical analysis of the pulp was; α-Cellulose, Klason Lignin, Hemicelluloses and Ash were 77.60 ± 0.65, 0.87 ± 0.23, 21.40 ± 0.76, and 1.30 ± 0.41%, respectively. All chemicals were obtained from Fluka and Aldrich without further purification.

### Methods

#### *Oxidation of cellulose to dialdehyde cellulose (DAC)*

In a water bath at 60 °C, 1.6 g of sodium metaperiodate ($NaIO_4$) was added to 2 g of cellulose suspended in water (1% consistency) and the reaction container was covered with aluminum foil to avoid the photo-induced decomposition of the periodate. After 5 h, ethylene glycol was added into the mixture to end the reaction by quenching the residual periodate. The oxidized cellulose (DAC) was thoroughly washed with alcohol followed by distilled water during the filtration. The aldehyde content which means the degree of oxidation was determined using hydroxylamine hydrochloride reacts with aldehyde group to generate hydrochloric acid (Kalmoush et al. 2020). The released hydrochloric acid was titrated with sodium hydroxide and the degree of oxidation was calculated from the following equation:

$$DO\,\% = \frac{MNaOH(V\ sample - V\ control)}{m/Mw} \times 100$$

where M is molarity of NaOH, m is the dry weight of the DAC sample (g), and Mw is the molecular weight of the repeating unit, $(C_6H_8O_{10})_n$, in DAC (160.124 g/mol).

#### *Preparations of heterocyclic derivatives*

(E)-2-(4-(dimethylamino)benzylidene)-4-oxo-4-phenylbutanehydrazide (a), (E)-2-((1,3-diphenyl-1H-pyrazol-4-yl)-4-oxo-4-phenylbutanehydrazide (b), and thiophene-2-carbohydrazide (c) were prepared according to a procedure previously reported in the

literatures (Abou-Elmagd et al. 2016; Khan and Rastogi 1991; Reid and Heindel 1976).

*Preparation of heterocyclic cellulose compounds*

To suspended solution of 1 g DAC in 10 mL a mixture of ethylene glycol/ DMSO (10:1) a heterocyclic compound as individual was added and homogenized for 2 min. In a sonication water path, the homogenate mixture was heated to 50 °C. After 1 h, the reaction product was washed several times with ethanol and frozen in a deep-freezer at − 80 °C followed by the freeze-drying process (ALPHA 1–2/LD PLUS, Martin Christ, Germany). The cellulose derivatives from the reaction of cellulose with (E)-2-(4-(dimethylamino)benzylidene)-4-oxo-4-phenylbutanehydrazide, (E)-2-((1,3-diphenyl-1H-pyrazol-4-yl)-4-oxo-4-phenylbutanehydrazide, and thiophene-2-carbohydrazide were taken the following code letters R, Y, and W respectively.

## Characterizations

Fourier transfer infrared spectroscopy (FT-IR)

The FT-IR spectra of native DAC, heterocyclic derivatives, as well as the prepared compounds were recorded with FT-IR spectrometer (Nicolet Impact-400 FT-IR spectrophotometer) in the range of 400–4000 $cm^{-1}$.

Surface morphology and EXD

The surfaces of the prepared samples were investigated by SEM coupled with energy dispersive X-ray analysis; Model Quanta 250 FEG (Field Emission Gun) attached with EDX Unit (Energy Dispersive X-ray Analyses) for EDX, with accelerating voltage 30 kV (Hashem et al. 2020a).

Thermo gravimetric analysis

The thermal stability of native DAC and prepared compounds were carried out using a TGA Perkin-Elmer (STA6000), with a heating rate (10 °C/min). The temperature ranged from room temperature up to 800 °C under air atmosphere (50 mL/min).

Antimicrobial activity

*Microbial strains and growth conditions*

Antimicrobial activity of heterocyclic cellulose compounds was assessed against seven microorganisms including Gram-negative bacteria (*Escherichia coli* ATCC25922 & *Pseudomonas aeruginosa* ATCC 27,853), Gram-positive bacteria (*Staphylococcus aureus* ATCC25923 & *Bacillus subtilis* ATCC6051), unicellular fungi (*Candida albicans* ATCC90028 & *Cryptococcus neoformance* ATCC 14,116), and multicellular fungi (*Aspergillus niger* RCMB 02,724 and *A. fumigatus* RCMB 02,568). Bacterial strains were cultured on nutrient agar at 37 °C for 24 h, while fungal strains were inoculated on malt extract agar (MEA) plates then incubated for 3–5 days at 28 ± 2 °C; and then kept at 4 °C for further use (Fouda et al. 2015; Hashem et al. 2019, 2020b; Khalil and Hashem 2018).

*Agar well diffusion method*

Agar well diffusion method was used for inhibition zone determination of tested heterocyclic cellulose compounds. The test of diffusion in agar was performed in accordance with the document M51-A2 of the Clinical Laboratory Standard Institute (Standards 2002) with minor adaptations. The selected bacterial strains were cultured on nutrient agar media for 24 h at 37 °C. Bacterial suspensions of $1.5 \times 10^6$ CFU/mL were separately prepared, seeded into Muller Hinton agar media, and poured aseptically into sterilized petri plates. 100 µL of the tested compound and standard antibiotic (Amoxicillin/clavulanate) at concentration 1 mg/mL was added in agar well, and then plates were put in refrigerator for 2 h followed by incubation at 37 °C for 24 h. While as, fungal strains were initially grown on MEA plates and incubated at 30 °C for 3–5 days (Suleiman et al. 2018a, 2018b). The fungal suspension was prepared in sterilized phosphate buffer solution (PBS) pH 7.0, and then the inoculums was adjusted to $10^7$ spores/mL after counting in a cell counter chamber. One mL was uniformly distributed on agar MEA Plates. Sterile cork borer (75 mm) was used for making well in inoculated MEA plates, and then 100 µl of the tested compound and reference antifungal (nystatin) at concentration 1 mg/mL was added. All MEA plates were incubated

at 30 °C for 72 h, and then the inhibition zone diameter was measured (Dacrory et al. 2021; Hashem et al. 2021a).

*Minimum inhibitory concentration (MIC)*

Three heterocyclic cellulose compounds (R, W, and Y), DAC as a start material, Amoxicillin Clavulanate (AMC) as a standard antibiotic and nystatin as a standard antifungal agent were prepared in different concentrations ranged from 1000 to 15.62 µg/mL, then assessed separately to detect MIC against selected bacterial and fungal strains (Hashem et al. 2021b; Valgas et al. 2007).

*In-vitro cytotoxicity and anticancer activity*

The cytotoxicity of DAC and the three heterocyclic cellulose compounds was determined using the MTT protocol (Khalil et al. 2020; Van de Loosdrecht et al. 1994) with minor modification. The normal Wi38 cell line, and two cancerous cell lines Hep G2 (liver hepatocellular carcinoma) and MCF7 (breast cancer) were collected from American type culture collection (ATCC). The cell quantity and the percentage of viable cell were totaled by the following formula:

$$\text{Viability}\% = \frac{\text{Test OD}}{\text{Control OD}} \times 100$$
$$\text{Cytotoxicity}\% = 100 - \text{Viability}\%$$

## Computational methodology

*System preparation*

The X-ray crystal structures of cKit tyrosine kinase was retrieved from the Protein Data Bank (PDB code: 1t46) (Mol et al. 2004). These structures were then prepared for molecular dynamics (MD) studies using UCSF Chimera (Pettersen et al. 2004). The missing residues were modeled using MODELLER 9.19 (Webb and Sali 2014) integrated with Chimera software. R and W compounds were drawn using Chem Bio Draw Ultra 12.1 (Reflections On Chem-Draw 2014). Hydrogen atoms were added to the ligand and removed from the receptor. Altogether, all three prepared systems were subjected to 50 ns MD simulations described in the simulation section.

*Molecular dynamic (MD) simulations*

The integration of Molecular dynamic (MD) simulations in biological systems' study enable exploring the physical motion of atoms and molecules that cannot be easily accessed by any other means (Hospital et al. 2015). The insight extracted from performing this sort of simulations provides an intricate perspective into the biological systems' dynamical evolution, such as conformational changes and molecule association (Hospital et al. 2015). The MD simulations of all systems were performed using the GPU version of the PMEMD engine present in the AMBER 18 package (Lee et al. 2018). Each compound's partial atomic charge was generated using ANTECHAMBER utilizing General Amber Force Field (GAFF) protocol (Wang et al. 2006). Each system was implicitly solvated within an orthorhombic box of TIP3P water molecules within 10 Å of any box edge, performed by the Leap module of the AMBER 18 package. Neutralization of each system was further implemented via $Na^+$ and $Cl^-$ counter ions integrated with the Leap module. An initial minimization of each system was performed for 2000 steps in the presence of an applied restraint potential of 500 kcal/mol, followed by a full minimization of 1000 steps carried out by conjugate gradient algorithm omitting restraints.

Each system was gradually heated during the MD simulation from 0 to 300 K for 500 ps, ensuring that all systems maintained a fixed number of atoms with a fixed volume. The system's solutes were imposed with a potential harmonic restraint of 10 kcal/mol and a collision frequency of 1 ps. Ensuing heating, equilibration of each system was performed for 500 ps at a constant temperature of 300 K. The number of atoms and pressure within each system for each production simulation were kept constant to mimic an isobaric-isothermal (NPT) ensemble, with the system's pressure being maintained at 1 bar using the Berendsen barostat (Berendsen et al. 1984).

Each system was MD simulated for 50 ns. In each simulation, the SHAKE algorithm was employed to constrain the hydrogen bond atoms. The step size of each simulation was 2 fs and integrating an SPFP precision model. The simulations coincided with an isobaric-isothermal ensemble (NPT), with randomized seeding, constant pressure of 1 bar, a pressure-coupling constant of 2 ps, a temperature of 300 K, and

Langevin thermostat with a collision frequency of 1 ps.

*Post-MD analysis*

The trajectories generated after MD simulations were each saved every 1 ps, followed by analysis using the CPPTRAJ (Roe and Cheatham III 2013) module implemented in the AMBER18 suite. All plots and visualizations were completed using the Origin (Seifert 2014) data analysis tool and Chimera (Pettersen et al. 2004), respectively.

*Thermodynamic calculation*

To estimate the binding interaction of the studied heterocyclic cellulose compounds toward the c Kit tyrosine kinase receptor, binding free energy was computed using molecular mechanics integrated with the Poisson-Boltzmann or generalized Born and surface area continuum solvation (MM/PBSA and MM/GBSA) approach (Genheden and Ryde 2015b). MM/GB-SA and MM/PB-SA rely on the ligand–protein complex molecular simulations to compute rigorous statistical-mechanical binding free energy within a specified force field (Drissi et al. 2015; Hayes and Archontis 2012b). Binding free energy averaged over 500 snapshots extracted from the entire 50 ns trajectory. The estimation of the change in binding free energy (ΔG) for each molecular species (complex, ligand, and receptor) can be represented as follows (Hou et al. 2010):

$$\Delta G_{\text{blind}} = G_{\text{complex}} - G_{\text{receptor}} - G_{\text{lignand}} \quad (1)$$

$$\Delta G_{\text{blind}} = E_{\text{gas}} + G_{\text{sol}} - \text{TS} \quad (2)$$

$$E_{gas} = E_{\text{int}} + E_{\text{vdw}} + E_{\text{ele}} \quad (3)$$

$$G_{\text{sol}} = G_{\text{GB}} + G_{\text{SA}} \quad (4)$$

$$G_{\text{SA}} = \gamma \text{SASA} \quad (5)$$

The term $E_{gas}$, $E_{int}$, $E_{ele}$, and $E_{vdw}$ symbolize the gas-phase energy, internal energy, Coulomb energy, and van der Waals energy, respectively. The $E_{gas}$ was directly assessed from the FF14SB force field terms. Solvation free energy ($G_{sol}$) was evaluated from the energy involvement from the polar states ($G_{GB}$) and non-polar states (G). The non-polar solvation free energy ($G_{SA}$) was determined from the Solvent Accessible Surface Area (SASA) (Sitkoff et al. 1994) using a water probe radius of 1.4 Å. In contrast, the polar solvation ($G_{GB}$) contribution was assessed by solving the GB equation. Items S and T symbolize the total entropy of the solute and temperature, respectively. Each residue contributes to the total binding free energy obtained at the predicted active site by carrying out per-residue energy decomposition at the atomic level using the MM/GBSA method in AMBER 18 (Genheden and Ryde 2015a; Hayes and Archontis 2012a).

## Results and discussion

### Chemistry

Periodate oxidation of cellulose yields dialdehyde cellulose (DAC) which is one of a promising functionalized cellulose due to its chemical structure can provide many possibilities for follow-up chemistry. Periodate oxidation is the selective oxidation of C2-C3 bonds of glucopyranose ring by periodate ions formed dialdehyde groups at these positions and the degree of oxidation depends on the oxidation conditions (Lindh et al. 2014). Consequently, cellulose can be modified with aromatic or aliphatic amines by Schiff-base formation (Scheme 1) (Lucia et al. 2019). In this work the degree of oxidation is 58%.

The chemical structure of cellulose was changed by periodate oxidation and examined by FTIR spectra. Figure 1A shows the FTIR spectra of DAC, the characteristic bands of DAC appeared in the 1730 and 880 $cm^{-1}$ regions assigned to the hemiacetal and hydrated form (Kim et al. 2017). The absorption bands of the compound at 1555 and 1115 $cm^{-1}$ were characterized by N–H deformation and C–N stretching vibrations. This confirmed that the multifunctional amines were successfully introduced into the oxidized cellulose (Han et al. 2010).

The FTIR spectra for the Schiff's base products revealed the existence of the characteristic vibrational band which are assigned to the (C=N) group at 1620–1625 $cm^{-1}$. Additionally, the appearance of new strong bending band for (N–H) at 1600 $cm^{-1}$ for derivative W. The absence of the band characteristic the carbonyl group indicates to the dehydration process to produce the furan moiety in R and Y

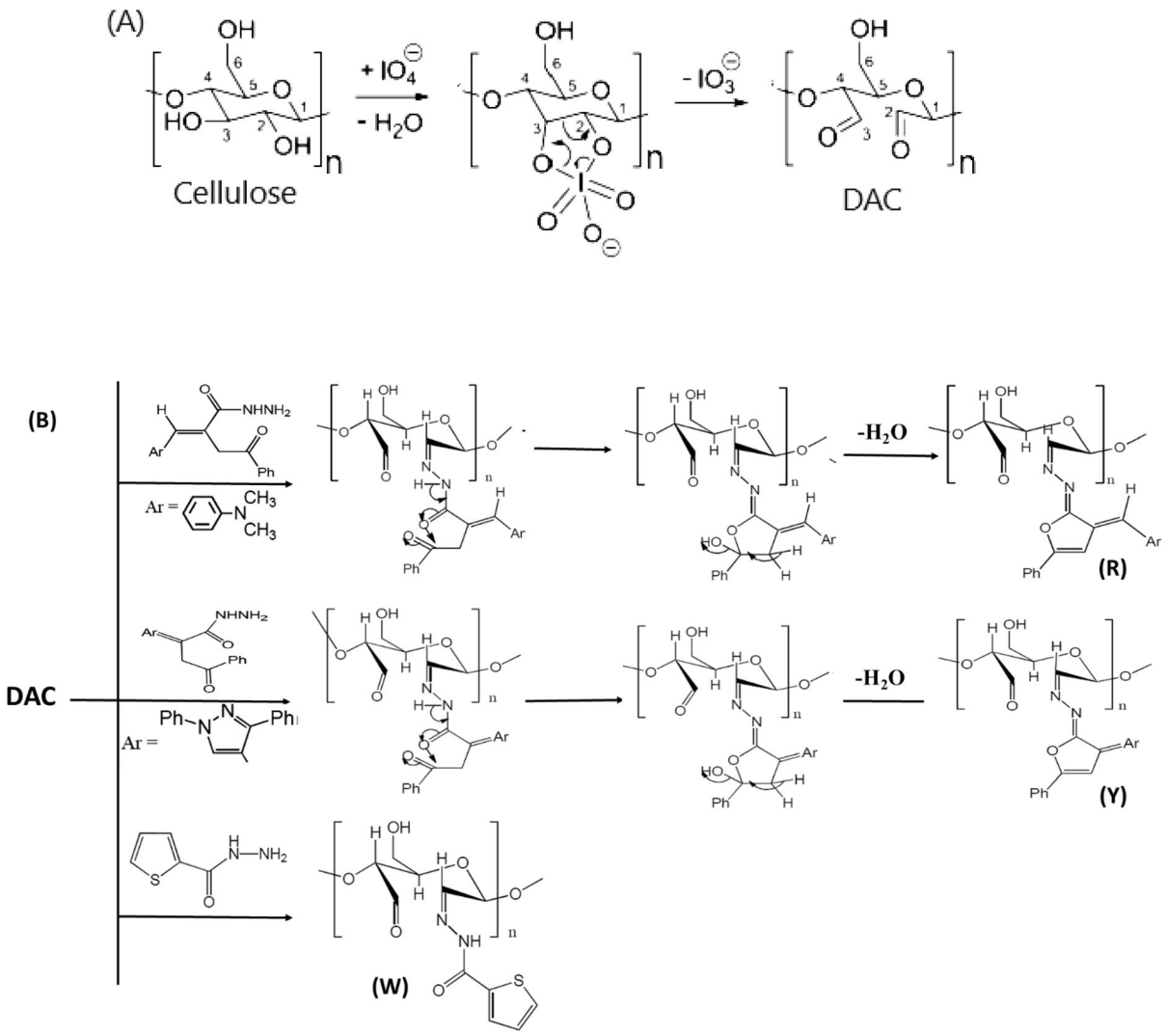


**Scheme 1** Plausible mechanism for periodate oxidation of cellulose (**A**) and the preparation of DAC derivatives (**B**)

derivatives. Consequently, the IR analysis for the products confirms that the reaction occurred through the formation of Schiff's bases between the active aldehyde group of DAC and the amino group of the heterocyclic cellulose compound (Abou-Elmagd et al. 2016; Hashem et al. 2017).

## Surface morphology by SEM

SEM micrographs of DAC, as well as its derivatives, proved that the formation of DAC by periodate oxidation of cellulose and the successive reaction of amines derivatives with DAC (Fig. 2). SEM image of DAC shows it is comprised of a smooth surface that lacked visible fibers and as reported in the literature, this confirms that the oxidation proceeded from the particle surface to the inside of the material and not only from the amorphous domains (Leguy et al. 2018). The formation of compact materials with smooth surfaces and no visible fibers has also been observed when DAC reacted with hetero derivatives.

Elemental compositions of DAC derivatives were studied by energy-dispersive X-ray spectroscopy (SEM–EDX) and are displayed in Fig. 2. Firstly, the

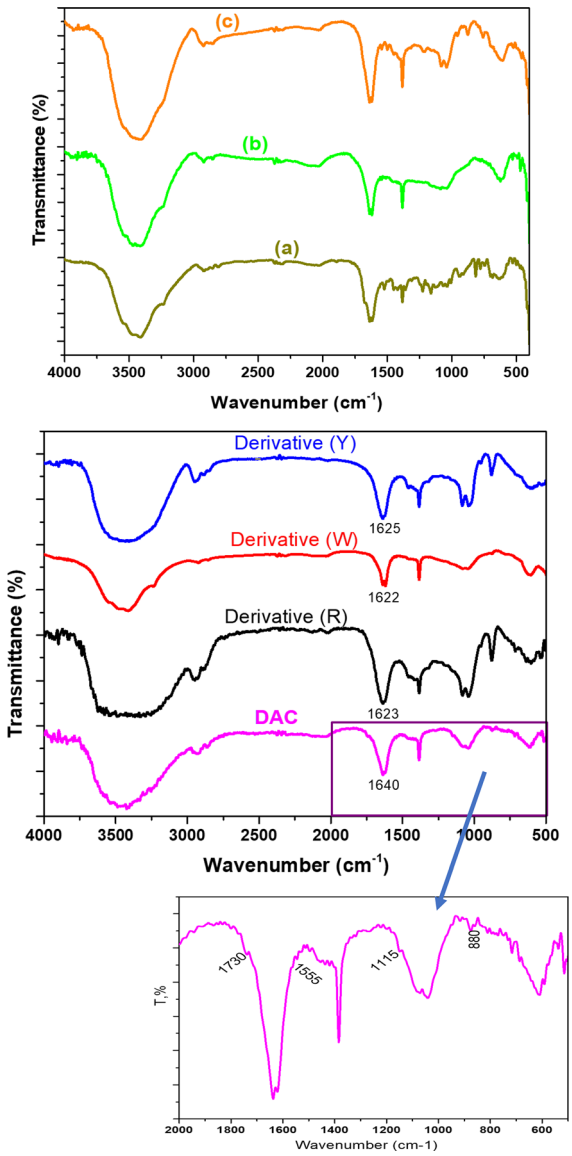


**Fig. 1** FTIR of neat heterocyclic materials (upper) and the native DAC as well as the prepared heterocyclic cellulose compounds (lower)

high nitrogen content observed for three DAC derivatives confirmed the efficient reaction of DAC with the heterocyclic derivatives (R, W, and Y). Another confirmation is the presence of sulfur in the EDX analysis of the W derivative.

## Thermal analysis

The TGA curves between 50 and 700 °C of DAC and its derivatives are depicted in Fig. 3. The degradation behavior of DAC showed significant differences from that of its derivatives. The first minor weight loss observed for DAC and its derivatives at 220 and 270 °C respectively, this attributed to dehydration such as physically adsorbed and hydrogen bond linked water molecules can be lost at this stage. The second stages of decomposition appeared at 309, 317, 320, and 336 °C for DAC and its derivatives R, Y, and W respectively. These results are emphasized that the reaction between DAC and heterocyclic derivatives occurred.

## Antimicrobial activity

Recently, heterocyclic cellulose compounds have been used as antimicrobial agents (Desai et al. 2018; Mustafa 2018). In the current study, compound R, W and Y which based on DAC and heterocyclic cellulose compounds were assessed their antimicrobial activity. Eight different fungal and bacterial strains were used in antimicrobial activity test. A comparison between the antimicrobial activity of R, W, and Y towards fungal and bacterial strains was carried out according to inhibition zone and MIC as shown in Fig. 4. The results revealed that, all designed derivatives exhibited antifungal and antibacterial activity toward all fungal and bacterial strains. Moreover, Y derivative was the highest for antimicrobial activity toward gram negative bacteria (*E. coli* and *P. aeruginosa*), unicellular fungi (*C. albicans* and *C. neoformance*) and multicellular fungi (*A. niger* and *A. fumigatus*) except gram positive bacteria (*B. subtilis* and *S. aureus*), while as DAC was the lowest against all strains. However, R derivative exhibited good antimicrobial activity toward all strains but it lower than Y derivative except *B. subtilis* and *S. aureus*. Individually, different concentrations for three designed derivatives, DAC, (Amoxicillin clavulanate)/(nystatin) as a standard antibacterial/antifungal were tested for antimicrobial activity to detect the minimum inhibitory concentration as shown in Fig. 4. EL-Sayed et al. (2017) proved that cellulose based 2-((2-aminoethyl)amino)-4-aryl-6-indolylnicotinonitriles have potential antimicrobial activity against gram positive bacteria and did not show any activity on gram negative bacteria. The

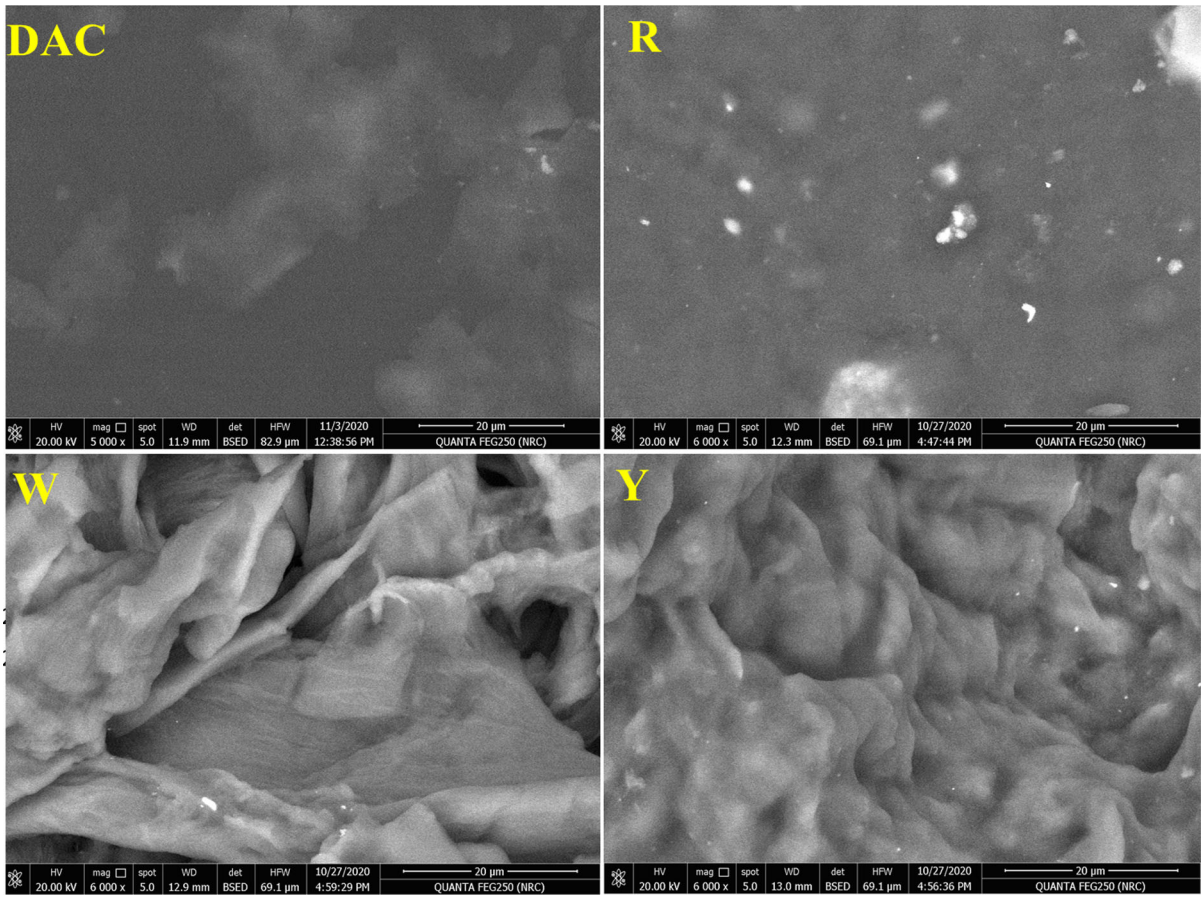


**Fig. 2** SEM image of DAC and SEM images as well as EDX analysis of R, W, and Y derivatives

results demonstrated that MIC of Y derivative against *E. coli, P. aeruginosa, B. subtilis, S. aureus, C. albicans* and *C. neoformance* was 62.5 µg/mL, while it was 31.25 µg/mL toward *A. niger* and *A. fumigatus*. However, MIC of R and W derivatives toward *E. coli, P. aeruginosa, C. neoformance* was 125 µg/mL, but MICs of R derivative against *B. subtilis, S. aureus, C. albicans, A. niger* and *A. fumigatus* were 62.5, 62.5, 125, 62.5 and 31.25 µg/mL respectively. Also, MIC of W derivative was 125 toward *B. subtilis, S. aureus, C. neoformance and A. fumigatus,* while as MICs of W derivative toward *C. albicans*and *A. niger* were 31.25 and 62.5 µg/mL. Generally, our designed heterocyclic cellulose derivatives exhibited good antimicrobial activity more than standard antibacterial/antifungal (AMC/nystatin) compounds. Eventually, these results concluded that quit low concentrations of three derivatives Y, R, and W (31.25–125 µg/mL) exhibited potential antimicrobial activity against gram positive, gram negative bacteria, unicellular and multicellular fungi.

## Antitumor activity

The cytotoxic effect of DAC, heterocyclic cellulose derivatives was determined against Wi38 by estimating the concentration for each compound ($IC_{50}$) at 50% cell viability. Figure 5A revealed that, $IC_{50}$ for all derivatives were more than 200 µg/mL. Generally, if the $IC_{50}$ is $\geq$ 90 µg/mL, the compound is classified as not cytotoxic (Ioset et al. 2009). Based on the above-mentioned results, heterocyclic cellulose derivatives did not display a significant toxicity to Wi38 cell line.

In vitro antitumor activity against Hep G2 and MCF cell lines at different concentrations (31.25–1000 µg/

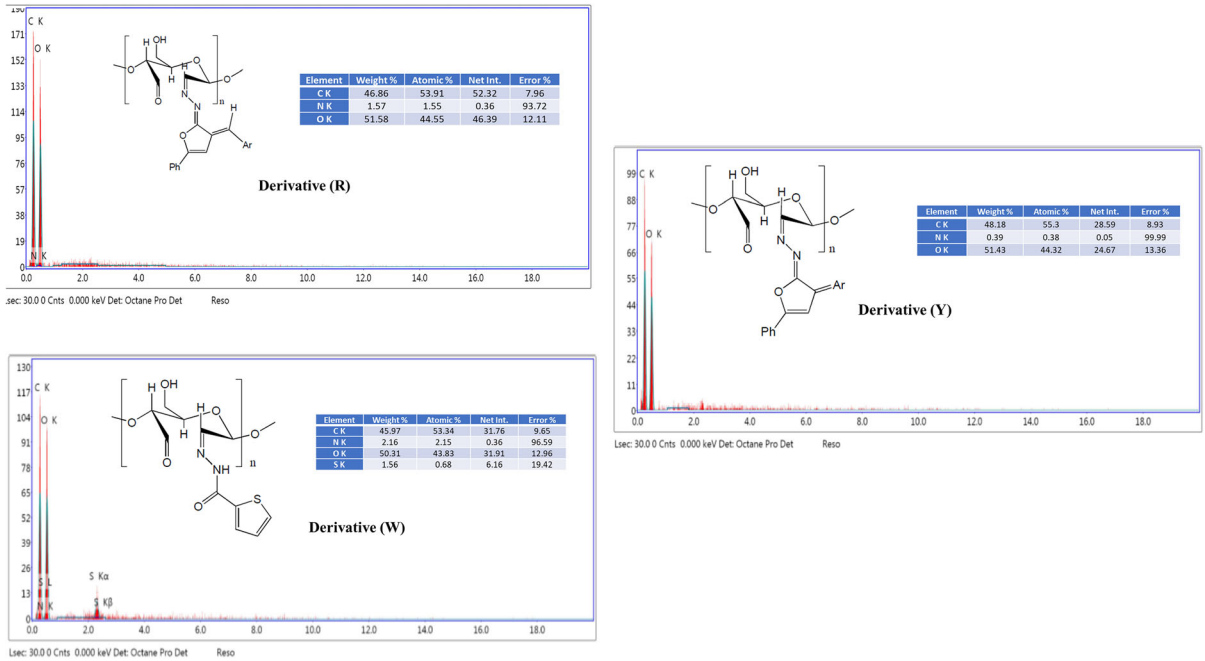


**Fig. 2** continued

mL) was assessed as shown in Fig. 5. The results revealed that, Y derivative was the highest for antitumor activity against cancerous cell lines Hep G2 and MCF, where concentrations above 100 µg/mL exhibited inhibition rate for both cancerous cell lines more than 50%. Moreover, R and W derivatives had antitumor activity against Hep G2 and MCF7 but lower than Y derivative. The compound Y caused a remarkable decrease in the development of tumor Hep G2 and MCF7, where the lethal concentrations of Y derivative which caused the death of 50% of human tumor Hep G2 and MCF7 were 90 and 102 µg/mL. Additionally, two derivatives R and W caused a decreasing in Hep G2 and MCF7 but lower than Y derivative, where $IC_{50}$ of R and W toward Hep G2 and MCF7 were (163 and 258) and (172 and 349 µg/mL) respectively. On the other hand, two derivatives Y and R have no effect on normal cell line Wi38 at these concentrations, but compound W has cytotoxic effect on Wi38 normal cell line at 349 µg/mL. Eventually, two compounds Y and R have good antitumor activities against Hep G2 and MCF7 tumor cell lines without any effects on Wi38 normal cell line. However compound W has antitumor activity but has cytotoxic effect on Wi38 normal cell line. In accordance with our results, recent studies proved antitumor activity of hetrocyclic compounds (Ali et al. 2018; Ismail and El-sayed 2019; Martins et al. 2015). Ismail and El-sayed (2019) screened fourteen heterocyclic compounds according to their antitumor activity against Hep G2 and MCF7 tumor cell line, and found all compounds had antitumor activity, and $IC_{50}$ in range 5.48–19.02 µM for all compounds. Moreover, Yusefi et al. (2020) loaded 5-Fluorouracil as a heterocyclic organic compound on cellulose fibers from rice straw and evaluated their antitumor activity, and reported the drug-loaded sample of CF/5-FU at a 250 µg/mL concentration inhibits colorectal cancer cells in ration 58%.

## Molecular dynamic (MD) and system stability

MD simulations were performed to investigate the inhibition efficiency and binding of the ligands within the catalytic active site. The validation of system stability is essential to trace disrupted motions and avoid artifacts during the simulation. The recorded average RMSD values for the entire systems were 2.00, and 1.63 Å for ckit- R and ckit- W derivatives respectively. The RMSD plot indicates that the cKit-W derivative system was more stable and convergence from the beginning of the simulation compared to the

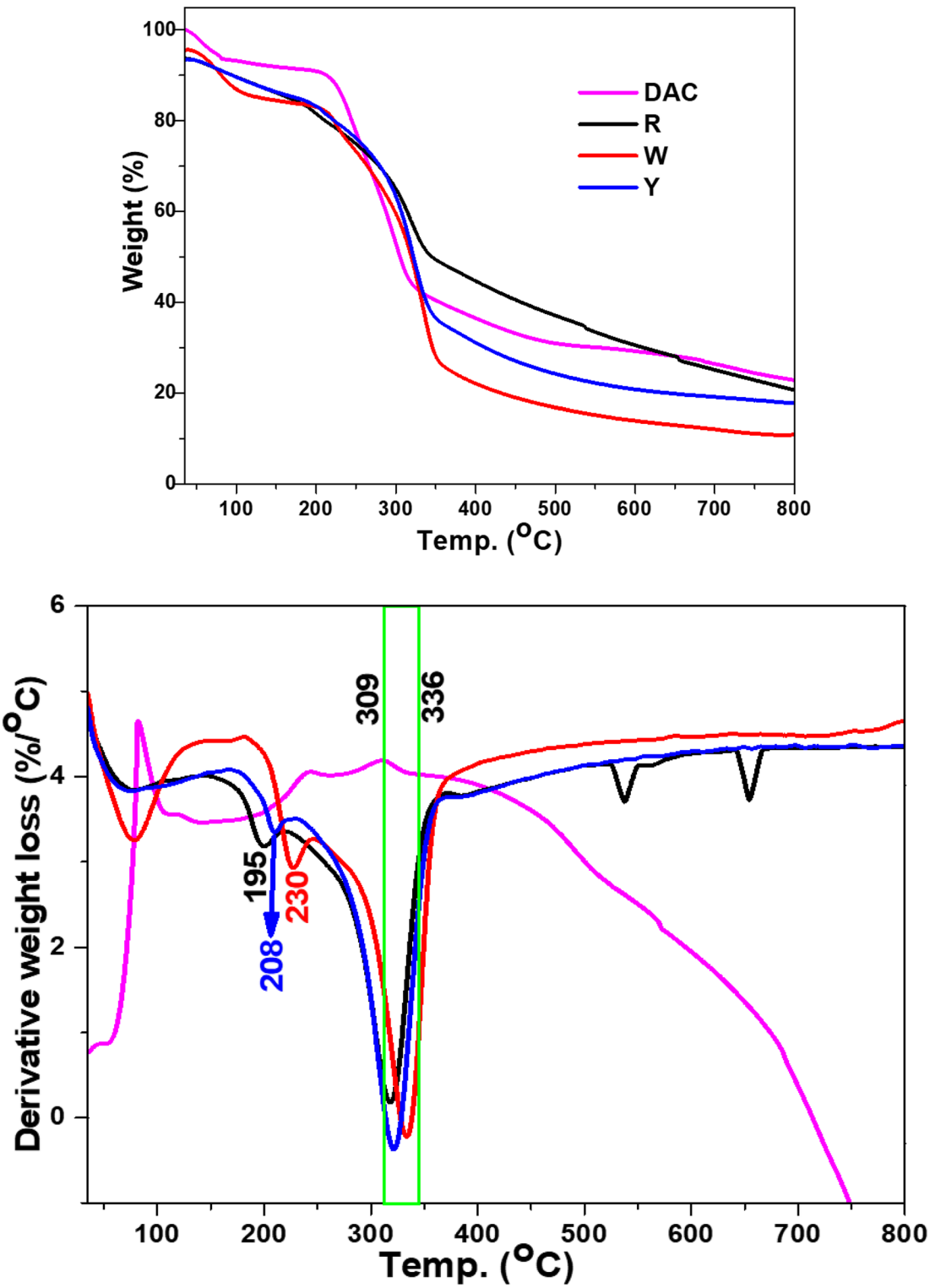


**Fig. 3** TGA (upper) and DTGA (lower) of DAC, R, W, and Y derivatives

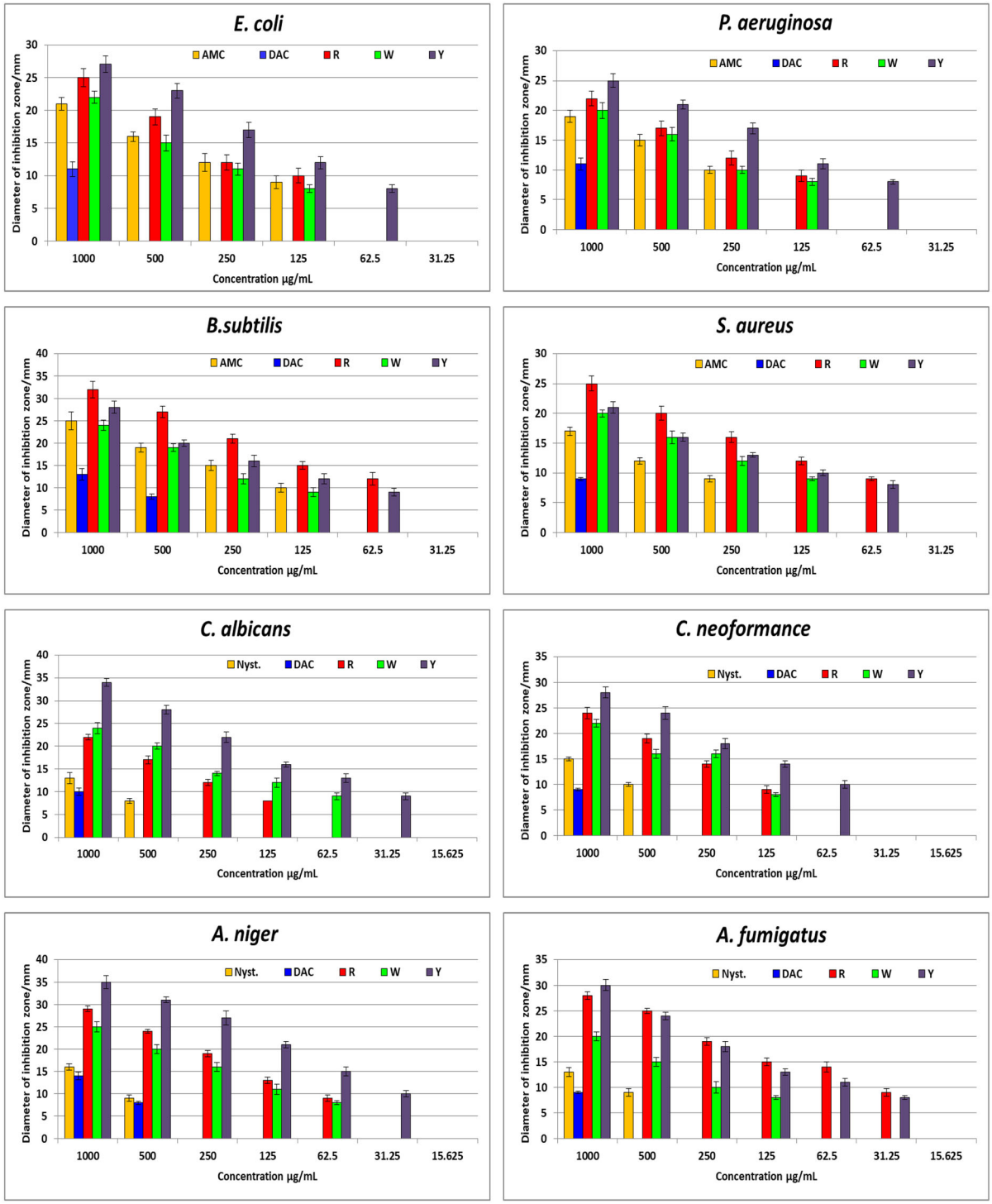


**Fig. 4** Antimicrobial activity and MIC of DAC, R, W, and Y compounds against *E. coli*, *P. aeruginosa, S. aureus*, *B. subtilis, C. albicans*, *C. neoformance*, *A. niger* and *A. fumigatus* (AMC = Amoxicillin Clavulanate and Nyst. = Nystatin)

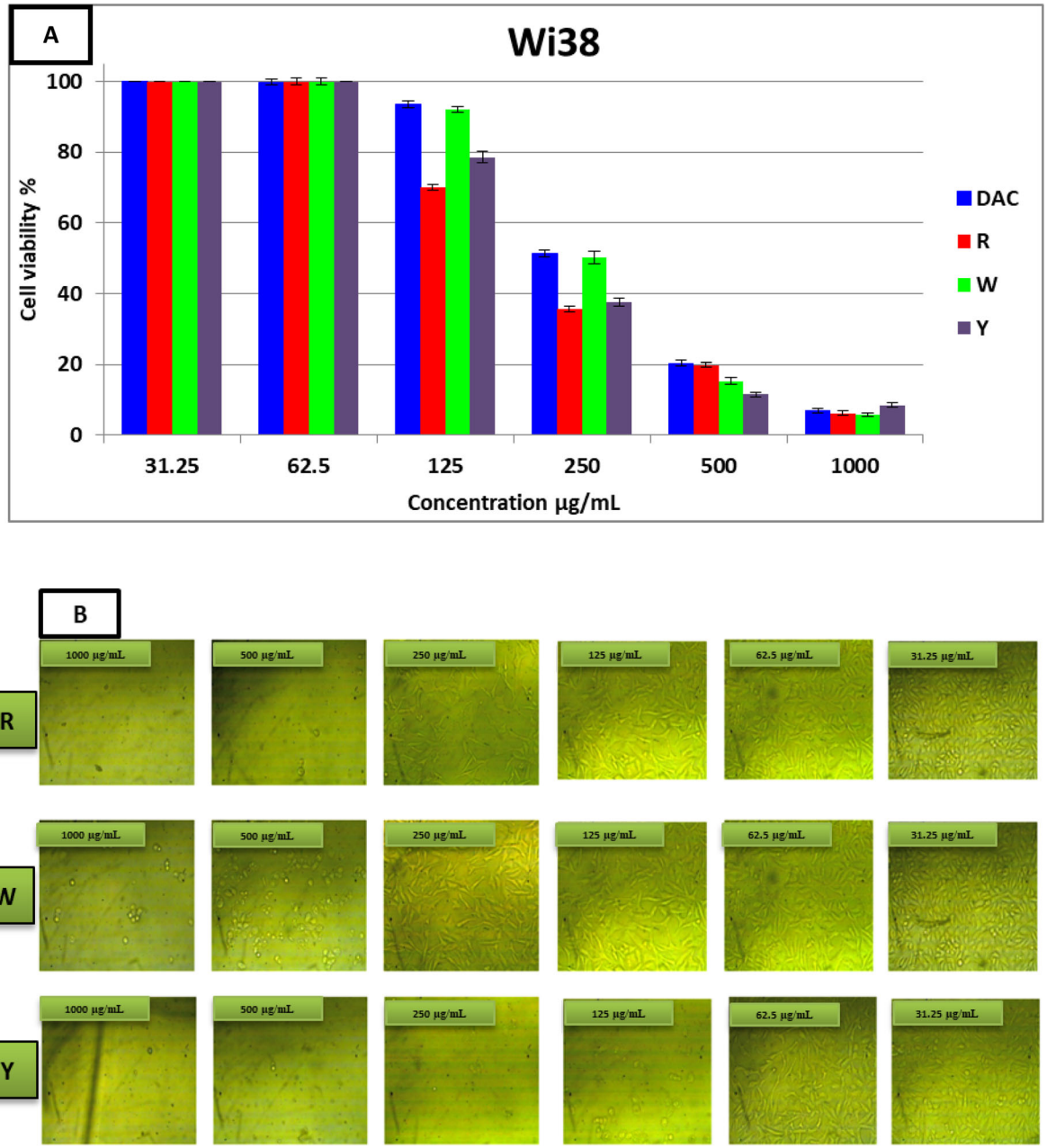


**Fig. 5** The cytotoxicity of DAC, R, W, and Y compounds against Wi38 normal cell line **A**. Antitumor activity of R, W, and Y derivatives against Hep G2 and MCF7 cancer cell line: Photos of treated Hep G2 **B** and MCF7 **D**; Inhibition rate % against Hep G2 **C** and MCF7 **E**

cKit-R derivative, which has been convergence 35 ns (Fig. 6A).

Afterward, we calculated the Root mean square fluctuation (RMSF) values to invest the R and W inhibitor's inhibitory effect towards the amino acid residues of the C kit receptor (Li et al. 2011). The computed average atomic fluctuation of Ckit-R and Ckit-W derivatives systems were 1.20 and 1.16 Å

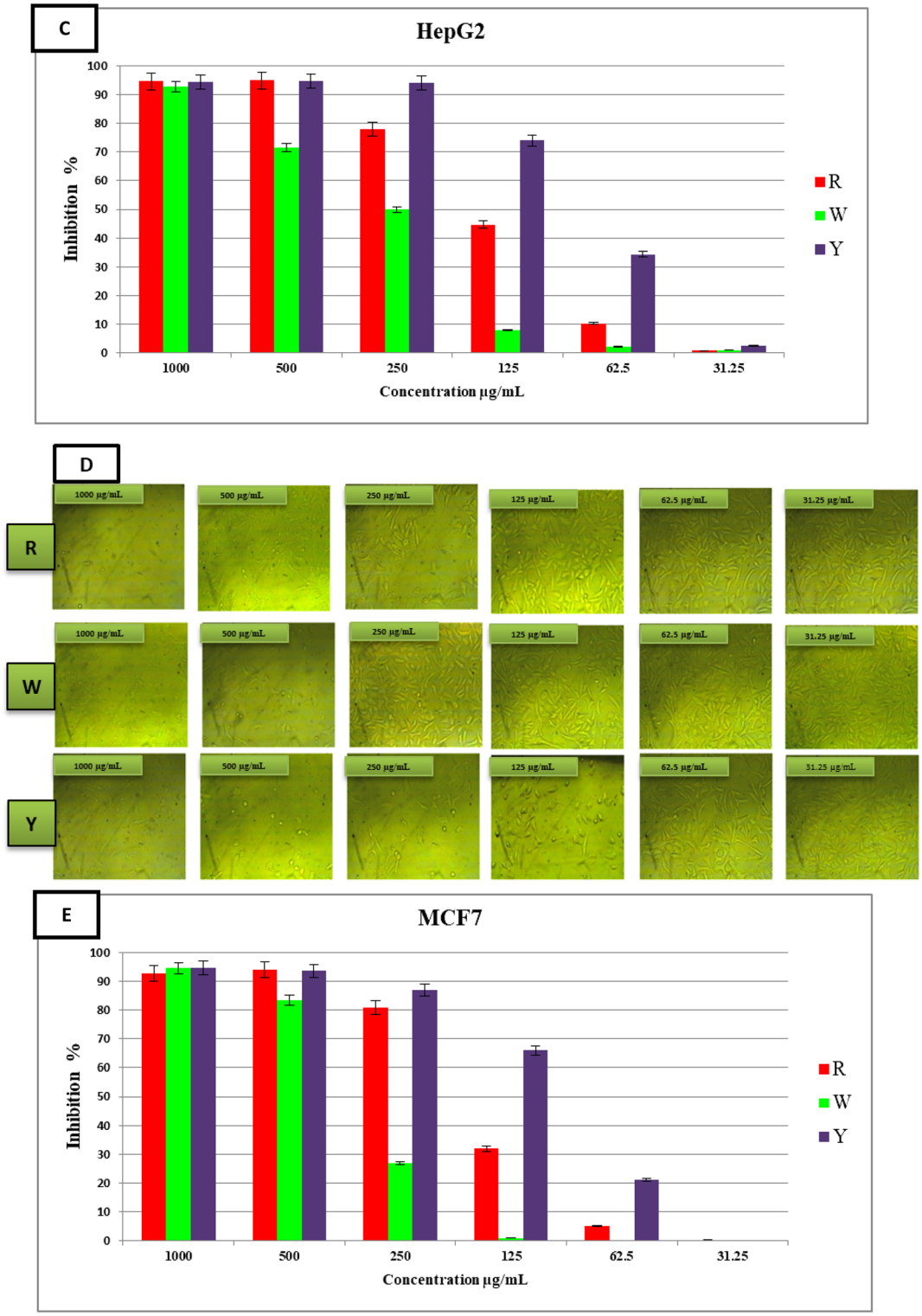


**Fig. 5** continued

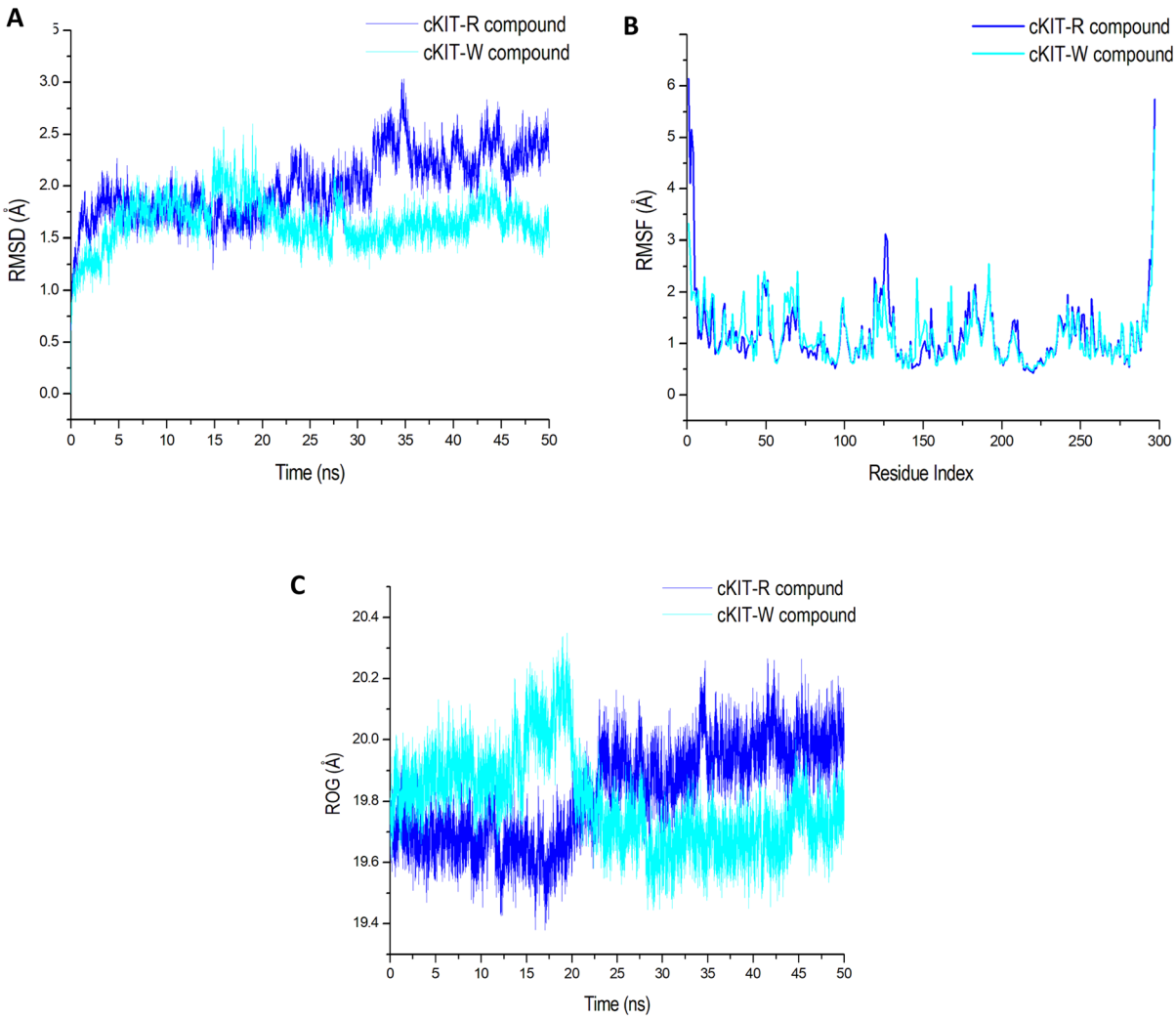


**Fig. 6** RMSD of Cα atoms of the protein backbone atoms (**A**), RMSF of each residue of the protein backbone Cα atoms (**B**). Radius of Gyration (ROG) of Cα atoms of protein residues of the backbone atoms relative to the starting minimized over 50 ns for cKit-R compound,and cKit-W compound systems (**C**)

respectively (Fig. 6). This result indicated a higher residue fluctuation of Ckit-R compared to the Ckit-W derivative systems (Fig. 6B).

The radius of gyration was measured to measure the overall system compactness as well as stability during MD simulation after ligand binding. The computed average Rg values were 19.8 and 19.76 Å for cKit-R and cKit-W derivative systems respectively (Fig. 6C). The observed behaviour suggested that the Ckit-W derivative system exhibited a high rigid structure compared to the Ckit-R derivative system.

## Mechanism of binding interactions based on binding free energy calculation

The binding of a ligand to a specific pharmacological target provides the structural basis for that ligand's activity. Therefore, predicting protein–ligand binding affinities based on free binding free energy calculations is an attractive approach to discovering new protein inhibitors (Cournia et al. 2017). The MM-GBSA program in AMBER18 was used in calculating the binding free energies by extracting snapshots from

**Table 1** Summary of the energy binding calculated for R and W against cKit tyrosine kinase receptor

| Energy components | | | | | | | |
|---|---|---|---|---|---|---|---|
| Derivative | $\Delta E_{vdW}$ | $\Delta E_{elec}$ | $\Delta G_{gas}$ | $\Delta G_{GB}$ | $\Delta G_{SA}$ | $\Delta G_{solv}$ | $\Delta G_{bind}$ |
| R | − 50.79 ± 0.11 | − 9.82 ± 0.36 | − 60.61 ± 0.36 | 33.19 ± 0.36 | − 6.64 ± 0.011 | 26.55 ± 0.36 | − 34.06 ± 0.14 |
| W | − 45.70 ± 0.08 | 29.62 ± 0.15 | − 75.33 ± 0.13 | 42.92 ± 0.10 | − 6.50 ± 0.005 | 36.41 ± 0.10 | − 38.91 ± 0.08 |

$\Delta E_{vdW}$ = van der Waals energy; $\Delta_{Eele}$ = electrostatic energy; $\Delta G_{solv}$ = solvation free energy; $\Delta G_{bind}$ = calculated total binding free energy (kcal/mol)

the trajectories of the compounds. As shown in Table 1, all the reported calculated energy components (except $\Delta G_{solv}$ and $\Delta G_{GB}$) gave high negative values indicating favorable interactions. For cKit receptor interactions with R and W derivatives, binding free energy ($\Delta G_{bind}$) values of − 34.06 and − 38.91 kcal/-mol were obtained. This indicated a more favorable binding of W towards compared to the R derivative system. It is fascinating to observe that the calculated binding free energies gave a good order regarding the experimentally determined $IC_{50}$ values.

A close look at the individual contribution of energy reveals that the more positive van der Waals energy components drive both R, and W derivative interactions with the C kit enzyme, resulting in the observed binding free energies. Substantial binding free energy values were observed in gas phase for all the inhibition process with values up to − 135.94 kcal/mol (Table 1).

## Identification of the critical residues responsible for inhibitor binding

In order to gain further insights into key residues involved in the inhibition of cKit tyrosine kinase receptor, the total energy involved when R and W derivatives bind these enzymes was further decomposed into the involvement of each site residues. From Fig. 7, the major favorable contribution of R derivative to C-kit tyrosine enzyme is predominantly observed from residues Tyr 14 (− 4.963 kcal/mol), Lys 17 (− 9.839 kcal/mol), Leu 31 (− 9.256 kcal/-mol), Lys38 (− 9.012 kcal/mol), Thr 30 (− 6.33 kcal/mol), Val 39 (− 8.93 kcal/mol), Val 40 (− 10.04 kcal/mol), Leu 73 (− 12.96 kcal/mol), Leu 77 (− 9.359 kcal/mol), lys 78 (− 9.322 kcal/mol), Val 79 (− 7.931 kcal/mol), Leu 80 (− 14.56 kcal/-mol), Leu 157 (− 10.609 kcal/mol), Leu 163 (− 12.54 kcal/mol), Leu 164 (− 16.091 kcal/mol), Thr 165 (− 9.524 kcal/mol), Asp 174 (− 44.592 kcal/mol) and Leu 177 (− 9.635 kcal/mol).

On the other hand, the major favorable contributions of C kit tyrosine kinase inhibition by W derivative were predominantly observed from residues Glu 76(− 46.72 kcal/mol), Leu 77 (− 7.72 kcal/mol), Lys 78 (− 6.376 kcal/mol), Val 79 (− 7.222 kcal/-mol), Leu 80 (− 14.619 kcal/mol), Leu 83 (− 13.118 kcal/mol), Lys 142 (− 7.598 kcal/mol),

Gly 143 (− 8.424 kcal/mol), Leu 147 (− 13.009 kcal/mol), Asp 156 (− 48.54 kcal/mol), Leu 157 (− 10.844 kcal/mol), Lys 171 (− 7.103 kcal/mol), Asp 174 (− 45.549 kcal/mol), Leu 177 (− 7.285 kcal/mol), Lys 182 (− 6.74 kcal/-mol), Lys 190 (− 5.31 kcal/mol), Gly 191 (− 4.61 kcal/mol), Lys 198 (− 7.948 kcal/mol), and Thr 211 (− 9.424 kcal/mol).

## Molecular mechanism and ligand binding mode analysis

Figure 8 illustrated that the c Kit tyrosine kinase ATP catalytic binding site Asp 174 residue has established a hydrogen bond interaction with the oxygen atoms of the cellulose group in both R and W compounds. In addition, the pharmacophoric hot spot, His 154, formed van der Walls interaction with R compound

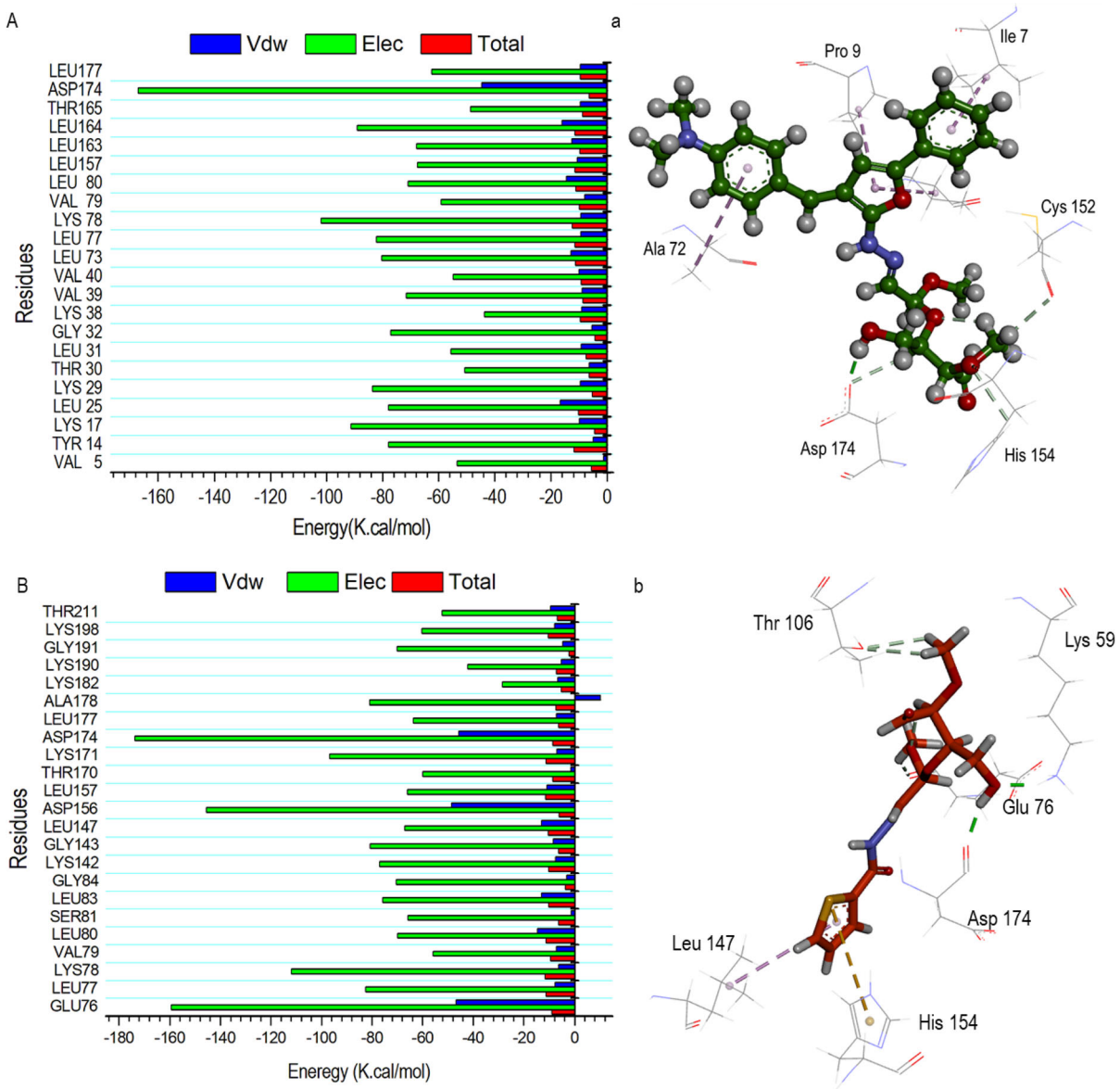


**Fig. 7** Per-residue decomposition plots showing the energy contributions to the binding and stabilization of R (**A**) and W (**B**) at the catalyatic active site of C kit tyrosine kinase receptor. Corresponding inter-molecular interactions are shown in R (a) and W (b)

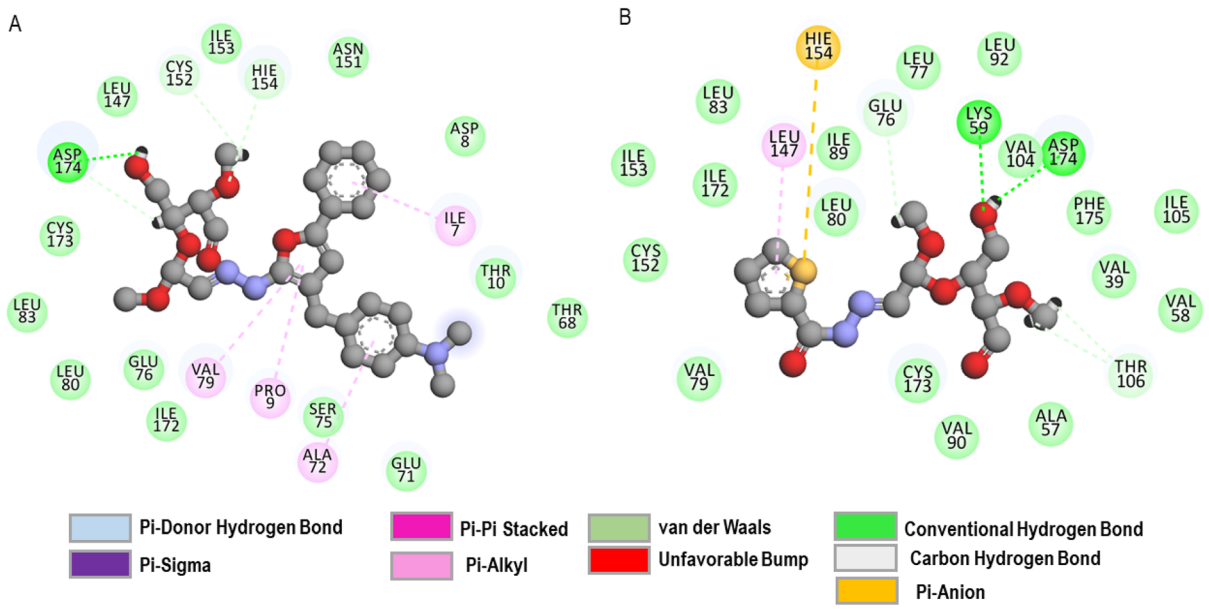


**Fig. 8** The key interactions between the cKit tyrosin kinase at the ATP binding site residues with R compound (**A**) and W compound (**B**)

and Pi -Anion interaction with W compound. It is noteworthy that five other hydrophobic- interacting residues were typical to both ligand; Ile 153, Lys 152, Glu 76, Val 79, and Leu 83 thus stabilizing both energetically favorable ligands in the hydrophobic pocket accessible. A total number of 21 residues were found at the binding interface of the cKit- R compound complex while 23 residues were seen in cKit-W compound interaction.

## Conclusion

Heterocyclic cellulose derivatives were prepared through the Schiff base reaction of oxidized cellulose (DAC) with amino heterocyclic derivatives. The reaction was elucidated by different analysis techniques and the results prove the successful formation of Schiff base with heterocyclic derivatives. The prepared derivatives have a broad antimicrobial activity against gram-positive, negative bacteria, unicellular, and multicellular fungi. Also, they exhibited good antitumor activities against Hep G2 and MCF7 tumor cell lines without any effects on the Wi38 normal cell line. Differential binding of R compound and W compound to these protein targets was measured using the MM-GBSA method, which revealed favorable interactions with ΔG values of -34.06 and -38.91 kcal/mol, respectively. The calculated binding free energy of W compound was higher compared to the R compound. The binding free energy component analysis suggests that the major energy constituent driving the W compound activity was van der Waals energy component. The decomposition of the total energies into individual active site residue contributions revealed that the amino acids that contribute largely to the inhibitor binding to c Kit tyrosine kinase are Glu76(− 46.72 kcal/mol), Leu77 (− 7.72 kcal/mol), Lys 78 (− 6.376 kcal/mol), Val 79 (− 7.222 kcal/mol), Leu 80 (− 14.619 kcal/mol), Leu 83 (− 13.118 kcal/mol), Lys 142 (− 7.598 kcal/mol), Gly 143 (− 8.424 kcal/mol), Leu 147 (− 13.009 kcal/mol), Asp 156 (− 48.54 kcal/mol), Leu 157 (− 10.844 kcal/mol), Leu 164 (− 16.091 kcal/mol), Lys 171 (− 7.103 kcal/mol), Asp 174 (− 45.549 kcal/mol), Leu 177 (− 7.285 kcal/mol), Lys 182 (− 6.74 kcal/mol), Lys 190 (− 5.31 kcal/mol), Lys 198 (− 7.948 kcal/mol), and Thr 211 (− s9.424 kcal/mol) are key components to the binding of cKit tyrosine kinase. Identification of these ATP binding site residues and their crucial roles could open a novel paradigm towards structure-based drug design of highly selective anti-tumor inhibitors

which would be considered in subsequent research from our group.

**Acknowledgments** The authors would like to acknowledge the support for this research from National Research Centre, Cairo, Egypt; and Faculty of Science, Al-Azhar University, Cairo, Egypt.

**Author contribution** MH research conceptualization, data curation, investigation, methodology, software, writing review and editing; AHH research conceptualization, data curation, investigation, methodology, software, writing review and editing; AAEl-R data curation, investigation, methodology, software, writing review and editing; SK research conceptualization, data curation, investigation, methodology, software, writing review and editing.

**Funding** All expenses whether chemical analysis or molecular identification etc. were funded by ourselves and there is no funder or funding agency support us to finish this work.

**Declarations**

**Conflict of interest** The authors declare that they have no conflict of interest.

## References

Abdelraof M, Hasanin MS, El-Saied H (2019a) Ecofriendly green conversion of potato peel wastes to high productivity bacterial cellulose. Carbohydr Polym 211:75–83

Abdelraof M, Hasanin MS, Farag MM, Ahmed HY (2019b) Green synthesis of bacterial cellulose/bioactive glass nanocomposites: Effect of glass nanoparticles on cellulose yield, biocompatibility and antimicrobial activity. Int J Biol Macromole 138:975–985

Abdelraof M, Ibrahim S, Selim MA, Hasanin M (2020) Immobilization of L-methionine γ-lyase on different cellulosicmaterialsand its potential application in green-selective synthesis of volatile sulfur compounds. J Environ Chem Eng 8:103870

Abou-Elmagd WS, EL-Ziaty AK, Elzahar MI, Ramadan SK, Hashem AI (2016) Synthesis and antitumor activity evaluation of some N-heterocycles derived from pyrazolyl-substituted 2 (3 H)-furanone. Synth Commun 46:1197–1208

Abu-Elghait M, Hasanin M, Hashem AH, Salem SS (2021) Ecofriendly novel synthesis of tertiary composite based on cellulose and myco-synthesized selenium nanoparticles: characterization, antibiofilm and biocompatibility. Int J Biol Macromole 175:294–303. https://doi.org/10.1016/j.ijbiomac.2021.02.040

Ali I, Mukhtar SD, Hsieh MF, Alothman ZA, Alwarthan A (2018) Facile synthesis of indole heterocyclic compounds based micellar nano anti-cancer drugs. RSC Adv 8:37905–37914

Berendsen HJ, Postma Jv, van Gunsteren WF, DiNola A, Haak J (1984) Molecular dynamics with coupling to an external bath. The Journal of chemical physics 81:3684-3690

Ciechanska D (2004) Multifunctional bacterial cellulose/chitosan composite materials for medical applications fibres. Text East Eur 12:69–72

Cournia Z, Allen B, Sherman W (2017) Relative binding free energy calculations in drug discovery: recent advances and practical considerations. J Chem Inf Modeling. 57:2911-2937 https://doi.org/10.1021/acs.jcim.7b00564

Dacrory S, Haggag ESA, Masoud AM, Abdo SM, Eliwa AA, Kamel S (2020) Innovative synthesis of modified cellulose derivative as a uranium adsorbent from carbonate solutions of radioactive deposits. Cellulose 27:7093–7108. https://doi.org/10.1007/s10570-020-03272-w

Dacrory S, Hashem AH, Hasanin M (2021) Synthesis of cellulose based amino acid functionalized nano-biocomplex: Characterization, antifungal activity, molecular docking and hemocompatibility Environmental Nanotechnology. Monitoring & Management 15:100453. https://doi.org/10.1016/j.enmm.2021.100453

de Coaña YP, Choudhury A, Kiessling R (2015) Checkpoint blockade for cancer therapy: revitalizing a suppressed immune system. Trends Mol Med 21:482–491

Desai N, Pandya D, Vaja D (2018) Synthesis and antimicrobial activity of some heterocyclic compounds bearing benzimidazole and pyrazoline motifs. Med Chem Res 27:52–60

Drissi M, Benhalima N, Megrouss Y, Rachida R, Chouaih A, Hamzaoui F (2015) Theoretical and experimental electrostatic potential around the m-nitrophenol molecule. Molecules 20:4042–4054. https://doi.org/10.3390/molecules20034042

El-Naggar ME, Hasanin M, Youssef AM, Aldalbahi A, Newehy M, Abdelhameed RM (2020) Hydroxyethyl cellulose/bacterial cellulose cryogel dopped silver@ titanium oxide nanoparticles: antimicrobial activity and controlled release of Tebuconazole fungicide. Int J Biol Macromole. https://doi.org/10.1016/j.ijbiomac.2020.09.226

EL-Sayed NS, El-Ziaty A, El-Meligy MG, Nagieb ZA (2017) Syntheses of New Antimicrobial Cellulose Materials Based 2-((2-aminoethyl) amino)-4-aryl-6-indolylnicotinonitriles. Egyptian J Chem 60: 465–477

Elbahnasawy MA, Shehabeldine AM, Khattab AM, Amin BH, Hashem AH (2021) Green biosynthesis of silver nanoparticles using novel endophytic Rothia endophytica: characterization and anticandidal activity. J Drug Delivery Sci Technol 62:102401

Felício MR, Silva ON, Gonçalves S, Santos NC, Franco OL (2017) Peptides with dual antimicrobial and anticancer activities. Front Chem 5:5

Fouda A, Khalil A, El-Sheikh H, Abdel-Rhaman E, Hashem A (2015) Biodegradation and detoxification of bisphenol-A by filamentous fungi screened from nature. J Adv Biol Biotechnol 2:123–132

Genheden S, Ryde U (2015a) The MM/PBSA and MM/GBSA methods to estimate ligand-binding affinities. Expert Opin Drug Discov 10:449–461

Genheden S, Ryde U (2015b) The MM/PBSA and MM/GBSA methods to estimate ligand-binding affinities. J Expert Opinion on Drug Discovery 10:449–461

Han S, Lee M, Kim BK (2010) Crosslinking reactions of oxidized cellulose fiber I reactions between dialdehyde cellulose and multifunctional amines on lyocell fabric. J Appl Polymer Sci 117:682–690

Hasanin M, El-Henawy A, Eisa WH, El-Saied H, Sameeh M (2019) Nano-amino acid cellulose derivatives: eco-synthesis, characterization, and antimicrobial properties. Int J Biol Macromole 132:963–969

Hasanin MS, Moustafa GO (2020) New potential green, bioactive and antimicrobial nanocomposites based on cellulose and amino acid International. J Biol Macromole 144:441–448

Hashem AH, Abdelaziz AM, Askar AA, Fouda HM, Khalil AMA, Abd-Elsalam KA, Khaleil MM (2021a) Bacillus megaterium-mediated synthesis of selenium nanoparticles and their antifungal activity against rhizoctonia solani in faba bean plants. J Fungi 7:195

Hashem AH, Hasanin MS, Khalil AMA, Suleiman WB (2019) Eco-green conversion of watermelon peels to single cell oils using a unique oleaginous fungus: lichtheimia corymbifera AH13. Waste and Biomass Valorization 1:5721

Hashem AH, Khalil AMA, Reyad AM, Salem SS (2021b) Biomedical applications of mycosynthesized selenium nanoparticles using penicillium expansum ATTC 36200. Biol Trace Element Res. https://doi.org/10.1007/s12011-020-02506-z

Hashem AH, Saied E, Hasanin MS (2020a) Green and eco-friendly bio-removal of methylene blue dye from aqueous solution using biologically activated banana peel waste. Sustainable Chem Pharm 18:100333

Hashem AH, Suleiman WB, Abu-elreesh G, Shehabeldine AM, Khalil AMA (2020b) Sustainable lipid production from oleaginous fungus syncephalastrum racemosum using synthetic and watermelon peel waste media. Bioresource Technol Reports 12:100569. https://doi.org/10.1016/j.biteb.2020.100569

Hashem AI, Abou-Elmagd WS, El-Ziaty AK, Ramadan SK (2017) Ring Transformation of a 2 (3H)-furanone derivative into oxazinone and pyrimidinone heterocycles. J Heterocyclic Chem 54:3711–3715

Hayes JM, Archontis G (2012a) MM-GB (PB) SA calculations of protein-ligand binding free energies. In: Molecular Dynamics-Studies of Synthetic Biological Macromolecules

Hayes JM, Archontis G (2012b) MM-GB (PB) SA calculations of protein-ligand binding free energies. In: Molecular Dynamics-Studies of Synthetic and Biological Macromolecules. IntechOpen,

Hoenich NA (2006) Cellulose for medical applications: past, present, and future. BioResources 1:270–280

Hospital A, Goñi JR, Orozco M, Gelpí JL (2015) Molecular dynamics simulations: advances and applications. J Advances applications in bioinformatics chemistry: AABC 8:37

Hou T, Wang J, Li Y, Wang W (2010) Assessing the performance of the MM/PBSA and MM/GBSA methods. 1 the accuracy of binding free energy calculations based on molecular dynamics simulations. J Chem Inf Model 51:69–82

Ioset J-R, Brun R, Wenzler T, Kaiser M, Yardley V (2009) Drug Screening for Kinetoplastids Diseases A Training Manual for Screening in Neglected Diseases

Ismail MF, El-sayed AA (2019) Synthesis and in-vitro antioxidant and antitumor evaluation of novel pyrazole-based heterocycles. J Iran Chem Soc 16:921–937

Kalmoush A, El-Sakhawy M, Kamel S, Salama A, Hesemann P (2020) A green method for preparation of amino acids functionalized 2, 3-dialdehyde cellulose Egyptian. J Chem 63:8–9

Kelloff GJ (1999) Perspectives on cancer chemoprevention research and drug development. Advances in cancer research. Elsevier, London, pp 199–334

Khalil A, Abdelaziz A, Khaleil M, Hashem A (2020) Fungal endophytes from leaves of Avicennia marina growing in semi-arid environment as a promising source for bioactive compounds. Lett Appl Microbiol 72:263–274

Khalil AMA, Hashem AH (2018) Morphological changes of conidiogenesis in two aspergillus species. J Pure Appl Microbiol 12:2041–2048

Khan R, Rastogi R (1991) A convenient and facile synthesis of 2-arylidene-4-phenylbut-3-en-4-olides by use of N, N-dimethyl (chlorosulphonyl) methaniminium chloride as a cyclodehydrating agent. J Chem Res Synopses (Print)

Kim U-J, Lee YR, Kang TH, Choi JW, Kimura S, Wada M (2017) Protein adsorption of dialdehyde cellulose-cross-linked chitosan with high amino group contents. Carbohyd Polym 163:34–42

Lee T-S et al (2018) GPU-accelerated molecular dynamics and free energy methods in Amber: performance enhancements and new features. J Chem Inf 58:2043–2050

Leguy J, Nishiyama Y, Jean B, Heux L (2018) Ultrastructural characterization of the core-shell structure of a wide range of periodate-oxidized cellulose from different native sources by solid-state 13C CP-MAS NMR. ACS Sustain Chem Eng 7:412–420

Li M-H, Luo Q, Xue X-G, Li Z-S (2011) Molecular dynamics studies of the 3D structure and planar ligand binding of a quadruplex dimer. J Mole Model. https://doi.org/10.1007/s00894-010-0746-0

Lindh J, Carlsson DO, Strømme M, Mihranyan A (2014) Convenient one-pot formation of 2,3-dialdehyde cellulose beads via periodate oxidation of cellulose in water. Biomacromol 15:1928–1932. https://doi.org/10.1021/bm5002944

Lucia A, van Herwijnen HW, Oberlerchner JT, Rosenau T, Beaumont M (2019) Resource-saving production of dialdehyde cellulose: optimization of the process at high pulp consistency. Chemsuschem 12:4679–4684

Martins P, Jesus J, Santos S, Raposo LR, Roma-Rodrigues C, Baptista PV, Fernandes AR (2015) Heterocyclic anticancer compounds: recent advances and the paradigm shift towards the use of nanomedicine's tool box. Molecules 20:16852–16891

Mol CD et al (2004) Structural basis for the autoinhibition and STI-571 inhibition of c-Kit tyrosine kinase. J Biol Chem 279:31655–31663

Mustafa YF (2018) Synthesis, characterization and antibacterial activity of novel heterocycle, coumacine, and two of its derivatives Saudi. Pharm J 26:870–875

Muthukumar T, Sambandam B, Aravinthan A, Sastry TP, Kim J-H (2016) Green synthesis of gold nanoparticles and their enhanced synergistic antitumor activity using HepG2 and MCF7 cells and its antibacterial effects. Process Biochem 51:384–391

Pettersen EF, Goddard TD, Huang CC, Couch GS, Greenblatt DM, Meng EC, Ferrin TE (2004) UCSF Chimera—a visualization system for exploratory research and analysis. J Comput Chem 25:1605–1612

Reflections on chemdraw. Chem Eng News Archive. https://doi.org/10.1021/cen-09233-scitech1

Reid JR, Heindel ND (1976) Improved syntheses of 5-substituted-4-amino-3-mercapto-(4H)-1, 2, 4-triazoles. J Heterocyclic Chem 13:925–926

Roe DR, Cheatham TE III (2013) PTRAJ and CPPTRAJ: software for processing and analysis of molecular dynamics trajectory data. J Chem Theory Comput 9:3084–3095

Seifert E (2014) OriginPro 9.1: scientific data analysis and graphing software software review. ACS Publications

Siegel RL, Miller KD, Jemal A (2015) Cancer statistics, 2015 CA: a cancer. J Clin 65:5

Sitkoff D, Sharp KA, Honig B (1994) Accurate calculation of hydration free energies using macroscopic solvent models. J Phys Chem 98:1978–1988

Standards NCfCL (2002) Reference method for broth dilution antifungal susceptibility testing of yeasts. National Committee for Clinical Laboratory Standards Wayne, PA,

Suleiman W, El-Sheikh H, Abu-Elreesh G, Hashem A (2018a) Recruitment of cunninghamella echinulata as an Egyptian isolate to produce unsaturated fatty acids. Res J Pharm Biol Chem Sci 9:764–774

Suleiman W, El-Skeikh H, Abu-Elreesh G, Hashem A (2018b) Isolation and screening of promising oleaginous Rhizopus Sp and designing of taguchi method for increasing lipid production. J Innov Pharma Biol Sci 5:8–15

Sung B, Prasad S, Yadav VR, Aggarwal BB (2012) Cancer cell signaling pathways targeted by spice-derived nutraceuticals. Nutr Cancer 64:173–197

Valgas C, Souza SMD, Smânia E, Smânia A (2007) Screening methods to determine antibacterial activity of natural products. Braz J Microbiol 38:369–380

Van de Loosdrecht A, Beelen R, Ossenkoppele g, Broekhoven M, Langenhuijsen M (1994) A tetrazolium-based colorimetric MTT assay to quantitate human monocyte mediated cytotoxicity against leukemic cells from cell lines and patients with acute myeloid leukemia. J Immunol Methods 174: 311-320

Wang J, Wang W, Kollman PA, Case DA (2006) Automatic atom type and bond type perception in molecular mechanical calculations. J Mole Graphics Modell 25:247–260

Webb B, Sali A (2014) Protein structure modeling with modeller. Protein Structure Prediction. Springer, NewYork, pp 1–15

Yusefi M et al (2020) The potential anticancer activity of 5-fluorouracil loaded in cellulose fibers isolated from rice straw. Int J Nanomed 15:5417